Korean J. Chem. Eng., 35(8), 1662-1672 (2018)
DOI: 10.1007/s11814-018-0074-0

pISSN: 0256-1115
eISSN: 1975-7220

A multipath peroxymonosulfate activation process over supported by magnetic $CuO\text{-}Fe_3O_4$ nanoparticles for efficient degradation of 4-chlorophenol

Wei Peng*, Jie Liu,†, Chenxu Li*, Fuxing Zong*, Wensi Xu*, Xing Zhang*, and Zhendong Fang**,†**

*Department of Graduate, Army Logistics University of PLA, Chongqing 401331, China
**Department of Military Facilities, Army Logistics University of PLA, Chongqing 401331, China
(*Received 4 April 2018 • accepted 2 May 2018*)

Abstract−Heterogeneous catalysts with low cost, environmentally friendly, highly effective and ready separation from aqueous solution are highly desirable. Magnetic $CuO\text{-}Fe_3O_4$ nanoparticles, a type of non-toxic bimetallic transition metal oxide, is a promising heterogeneous catalyst for activation of peroxymonosulfate (PMS) to generate reactive oxygen species (ROS) that has not been previously investigated. In this study, the activation of PMS by $CuO\text{-}Fe_3O_4$ nanoparticles was evaluated using the degradation of 4-chlorophenol as a model reaction. Several critical factors such as pH, catalyst dosage and PMS concentration were investigated. $CuO\text{-}Fe_3O_4$/PMS system demonstrated a wide effective pH range to degrade 4-chlorophenol, namely 5.5 to 9.5. With the increase of the catalyst dosage, the degradation efficiency of 4-chlorophenol appeared to increase first and then decrease, that the inflection point was 0.5 g/L. Elevated PMS concentration obviously improved the decomposition of 4-chlorophenol; however, the plateau was reached when the PMS concentration was 8 mM. Further increase in PMS concentration would not significantly improve the removal efficiency. Through examining the effects of scavengers and electron spin resonance (ESR) analyses, $CuO\text{-}Fe_3O_4$ nanoparticles were proven to activate PMS through a non-radical and radical pathway to generate singlet oxygen, sulfate radicals and hydroxyl radicals. Based on results, $CuO\text{-}Fe_3O_4$ nanoparticles were effective, environmentally friendly and low cost catalysts for efficient activation of PMS. These features make $CuO\text{-}Fe_3O_4$ nanoparticles a readily available heterogeneous catalyst to activate PMS for refractory organic pollutants degradation in advanced oxidation processes (AOPs).

Keywords: $CuO\text{-}Fe_3O_4$ Nanoparticles, Peroxymonosulfate, 4-Chlorophenol, Multipath Activation

INTRODUCTION

Chlorophenols (CPs) are important intermediates and raw materials for chemical industries, such as in the production of biocides, disinfectants, pesticides and dyes [1]. But chlorophenols are classified as priority toxic pollutant listed by the United States Environmental Protection Agency (USEPA), due to their high toxicity, long persistence and carcinogenic potential [2]. Thus, the removal of chlorophenols is of great significance for environmental protection.

However, effective degradation of refractory organic pollutants (ROPs) such as chlorophenols can be hardly achieved by conventional wastewater treatment technology due to their stable chemical structure [3]. Recently, advanced oxidative processes (AOPs) based on highly reactive oxygen species (ROS) have been proposed as an emerging and efficient method for the degradation of ROPs in wastewater [4,5]. Among the various AOPs, the activation of peroxymonosulfate (PMS) has received much attention because ·OH (1.9-2.7 V) and $\cdot SO_4^-$ (2.5-3.1 V) have high standard redox potentials [6,7].

Indeed, PMS has an asymmetric structure that makes it more readily activated than persulfate (PS) and hydrogen peroxide (H_2O_2), which have symmetrical structures [8]. PMS has been considered as inexpensive oxidant for remediation of contaminated water or soil. At present, PMS is commonly activated by heterogeneous catalysts (transition metal oxides and nonmetal catalysts), energy (heating, ultraviolet and ultrasound) and chemical regent (base) [9-13]. Considering the wide application, energy and chemical regent method is limited due to their high cost and energy input. Employment of heterogeneous catalysts is a promising alternative for PMS activation [14-16]. Shukla et al. [17] recently investigated activated carbon (AC) supported Co catalysts for phenol degradation and found that Co/AC exhibited high activity in oxidation of phenol with $\cdot SO_4^-$ and 100% decomposition, and 80% TOC removal could be achieved in 60 min. Saputra's group [18] has focused on synthesizing three one-dimensional MnO_2 nanoparticles with different crystallographic phases (α-, β- and γ-MnO_2) and tested in heterogeneous activation of PMS for phenol degradation in water. The α-MnO_2 nanowires exhibited the highest activity and phenol degradation achieved 100% at 20 min. Also, α-MnO_2 exhibited high stability in reuse tests without losing activity. Carbon-based material as a catalyst was also used for activation of PMS to generate free radicals [19]. Saputra et al. [20] applied activated carbon (AC) for activation of PS, H_2O_2 and PMS. It was observed that AC was effective in heterogeneous activation of PMS to produce $\cdot SO_4^-$ for degradation of phenol, much better than PS and H_2O_2. However, some researchers claimed that the durability of carbocatalysts was poor. Shao et al. [21] first discovered that amorphous boron could be used as a metal-free cata-

†To whom correspondence should be addressed.
E-mail: fzdhg123@126.com, liujiezxsh@hotmail.com

lyst for PMS activation for effective degradation of bisphenol S. Amorphous boron exhibited outstanding catalytic activity and superior stability as compared to other heterogeneous catalysts. In case of PMS activation, transition metal oxides were the most commonly used heterogeneous catalysts. Copper oxide (CuO) and ferroferric oxide (Fe_3O_4) are common transition oxides used in PS and PMS heterogeneous activation [22-24]. Zhang et al. [25] suggested that CuO could effectively activate PS under mild conditions without producing unselective $\cdot SO_4^-$, in which the decomposing 2,4-dichlorophenol (2,4-DCP) was contributed primarily by the outer-sphere interaction between PS and CuO. But Zhang's study did not mention the problem of the recovery of the catalyst. Ji et al. [26] found that CuO had a highly catalytic activity to degrade phenol in the presence of PMS. Quenching experiment showed that CuO effectively catalyzed the decomposition of PMS into ·OH and $\cdot SO_4^-$. However, the study conducted by Ji did not solve the problem of recovery of CuO and leaching problem of copper ion. Moreover, research has shown that Fe_3O_4 plays an important role in heterogeneous catalysis for PS and PMS because of its magnetic properties and ease of obtaining. Avetta et al. [27] suggested that phenol could be effectively degraded by Fe_3O_4 in the presence of PS under UVA irradiation. The degradation process involves the radical $\cdot SO_4^-$, formed from PS in the presence of Fe (II). Liu et al. [28] showed that the combination of Fe_3O_4 and ultrasound irradiation could significantly enhance the removal efficiency of Acid Orange 7 in which reaction involves ·OH and $\cdot SO_4^-$. The above studies show that Fe_3O_4 has a weak catalytic activity to active PS or PMS, which often needs the extra aid of ultrasonic sound and ultraviolet light. Obviously, the introduction of external energy increases the cost of the treatment process. Alternatively, an efficient way to overcome the drawbacks of the weak catalytic activity of Fe_3O_4 and poor recoverability of CuO is to combine CuO with Fe_3O_4, which might simultaneously utilize the high catalytic property of CuO and the magnetic property of Fe_3O_4. Very recently, CuO-Fe_3O_4 nanoparticles has been used to activate PS to degrade phenol [29]. The results showed that the new catalyst had good magnetic separation and catalytic properties and involved in sulfate radical reaction. However, the mechanism of PMS activated by CuO-Fe_3O_4 nanoparticles and the effect of CuO-Fe_3O_4/PMS system on the removal of ROPs has not been clearly illustrated.

In recent years, heterogeneous catalysts have been utilized to activate PMS for 4-chlorophenol degradation. Liu et al. [30] first synthesized magnetic Fe_3O_4-MnO_2 core-shell nanocomposites for decomposition of PMS to oxidize 4-CP. They reported that Fe_3O_4-MnO_2 (Fe/Mn molar ratio was 4) nanocomposites showed high capacity for heterogeneous activation of PMS and similar 100% 4-CP removal could be achieved in 30 min. However, according to the analysis of the obtained results, the success rate of synthesis of core-shell structure was not ideal which was not conducive to its popularization and application. Barzegar et al. [31] investigated the ultrasound (US)/PMS/nanoscale-zero valent iron (nZVI) process to degrade 4-CP. In their work, under the condition of pH=3.0, applying 0.4 g/L nZVI, 1.25 mM PMS and 200 W US power brought about 95% 4-CP removal in 30 min. However, the problem of Barzegar's research is that the catalyst (nZVI) synthesis method was complex, the optimal pH was acidity and the energy consumption was relatively large, which made the reaction process seem less green and less environmentally friendly. Guo et al. [32] applied S-doped activated carbon (ACS) for the activation of PS. As they have stated, ACS exhibited excellent catalytic activity for PS activation and a complete 4-CP degradation as well as 65.3% COD removal was achieved in 170 min at 25 °C with ACS dosage of 0.1 g/L, PS/4-CP molar ratio of 24/1 and the initial pH of 4.4. It could be found from Guo's work that although 4-CP was completely degraded, the treatment cycle was relatively long and pH needed to be adjusted after the end of the reaction, and the recovery of the catalyst was not mentioned. Therefore, it was particularly important to develop a heterogeneous catalyst with simple synthesis, high catalytic activity, easy separation and easy popularization and application. CuO-Fe_3O_4 nanoparticles mentioned above might have the above advantages. Whether the magnetic CuO-Fe_3O_4 nanoparticles could be used for PMS activation to degrade 4-CP still needed be further studied.

In this work, magnetic CuO-Fe_3O_4 nanoparticles were tested in improving PMS oxidation of a model refractory organic pollutant, 4-chlorophenol (4-CP). Then, the performance of CuO-Fe_3O_4 for the degradation of 4-CP was evaluated and several critical factors were investigated. Further, the involved mechanisms of the PMS activation by magnetic CuO-Fe_3O_4 nanoparticles were tentatively proposed. In particular, electron spin resonance (ESR) technique was employed to identify and discern the radical species produced in the CuO-Fe_3O_4/PMS system.

MATERIALS AND METHODS

1. Materials

All chemicals used were analytical grade and purchased from Sinopharm Chemical Reagent Co. Ltd. (Beijing, China). The 4-chlorophenol (purity>99.99%) and Oxone (PMS, $KHSO_5 \cdot 0.5KHSO_4 \cdot 0.5K_2SO_4$) were obtained from Sigma-Aldrich Co. Ltd. (Shanghai, China). The spin trapping reagent 5,5-dimethyl-pyrroline-oxide (DMPO) and 2,2,6,6-tetramethyl-4-piperidinol (TEMP) were supplied from Tokyo Chemical Industry Co. Ltd. All stock and fresh solutions were prepared with deionized water. Deionized (DI) water was obtained from a Milli-Q System (Millipore). The feed water temperature was 283 K and the resistivity of product water 18.2 MΩ·cm at 298 K.

2. Synthesis of Catalysts

The CuO-Fe_3O_4 catalyst was fabricated using a simple and one-step hydrothermal method, according to the following procedure [33]: Ferrous sulfate ($FeSO_4 \cdot 7H_2O$, 1.668 g) and copper chloride ($CuCl_2 \cdot 2H_2O$, 0.051 g) were dissolved in 100 mL deionized water at a Fe/Cu molar ratio of 20 : 1. The solution was stirred magnetically for 10 min, and then 1 g Poly (vinylpyrrolidone) (PVP, K-30) was added. Under magnetic stirring, 5 M sodium hydroxide (NaOH) solution was added to adjust the mixture solution pH to around 10-11. After addition of alkali, the suspension formed was continuously stirred for 4 h at 363 K water bath, aged at room temperature for 10 h, and then washed several times with ethanol and deionized water till alkali and PVP free. The mass fraction of CuO in the synthesized composite was 5%. The obtained material appeared as fine powder and was dried in a vacuum oven at 393 K for 12 h.

Finally, the dry material was stored in a desiccator for further use. Catalysts with different copper oxide content could be synthesized according to the above method.

The CuO catalyst was fabricated using a one-step hydrothermal method, according to the following procedure: Solution containing ($CuCl_2 \cdot 2H_2O$, 1.023 g) and PVP (1.0 g) was added into 100 mL DI water heated to 363 K. After that, NaOH solution (5 M, 3 mL) was added into the mixture. The produced precipitate was aged within mother liquid for 2 h under 363 K. The solid powders were separated by centrifugation and washed several times by using DI water and ethanol, followed by drying at 393 K in a vacuum drying oven.

The Fe_3O_4 catalyst was fabricated using a one-step hydrothermal method, according to the following procedure: Solution containing ($FeSO_4 \cdot 7H_2O$, 1.668 g) and PVP (1.0 g) was added into 100 mL DI water heated to 363 K containing 0.02 mol NaOH under magnetic stirring. The produced precipitate was aged within mother liquid for 4 h under 363 K. The solid powders were separated by external magnetic field and washed several times by using DI water and ethanol, followed by drying in a vacuum oven at 333 K for 4 h.

3. Characterization of Catalysts

The crystal phase of the synthesized materials was detected on an X-ray diffractometer (Smartlab9, Rigaku, Japan) operated at 40 kV and 30 mA with Cu/Kα radiation with 2θ ranging from 10° to 80°. The morphology of the synthesized nanoparticles was examined by scanning-electron microscope coupled to energy dispersive spectrometer (SEM-EDS, Hitachi S-3500N, Japan), transmission electron microscopy (TEM, JEOL-2010, Japan) and high resolution TEM (HRTEM). A vibrating sample magnetometer (VSM, JDM-13, China) was applied to determine the magnetic properties of the synthesized materials. The isoelectric point (pH at the point of zero charge, pH_{pzc}) of the catalysts was analyzed through a Malvern Zeta potentiometer (Zetasizer WT, Malvern Panalytical, U.K).

4. Experimental Operations

Catalytic degradation experiments were conducted in 250 mL brown conical flasks. The brown conical flasks containing aqueous solution were agitated on a reciprocating shaker at 150 rpm and 303 K in dark. Tetra-borate was used as a buffer in most of the reactions, because phosphate is a strong coordinate for transition metal. Predetermined volumes of 4-CP solution were injected into DI water to get the desired initial concentration and then the specific dose of sonicated nanoparticles were introduced into the prepared solution. The obtained mixture was agitated for 10 min to maintain the adsorption/desorption equilibrium between catalyst and contaminants before the oxidant solution addition. Samples withdrawn at different time intervals were mixed with 20 μL sodium thiosulfate solution to quench the Oxone solution, and then immediately filtered through 0.22 μm glass fiber filters into a high performance liquid chromatograph (HPLC) vial for 4-CP analysis. The filtration had no impact on the 4-CP concentration. For the successive repeated reaction, the catalyst was separated by external magnetic field after the reaction was completed and washed with DI water and ethanol to neural pH. And then the catalyst was dispersed in 100 mL solution containing the same concentration of 4-CP, Oxone and tetra-borate. All experiments were conducted in triplicate and the results were reproducible within the experiments errors (±5%).

Quenching experiments were performed to determine the radical species formed in the $CuO\text{-}Fe_3O_4$/PMS system by using *tert*-butanol, methanol and furfuryl alcohol as a quenching agent of ·OH, $\cdot SO_4^-$ and single oxygen ($^1O_2$) [34]. Prior to the addition of $CuO\text{-}Fe_3O_4$, a specific amount of the quencher was added into the reaction solution.

The settings for the ESR spectrometer (A300 spectrometer, Bruker, U.S) were listed as follows: sweep width at 100 G, microwave frequency at 9.77 GHz, modulation frequency at 100 kHz, modulation amplitude at 1.00 G, power at 20.00 mW.

5. Analysis

4-CP analysis was performed on an Agilent HPLC equipped with a UV detector at λ=280 nm and C18 reversed-phase column (250×3.0 mm). The mobile phase used for HPLC experiments was a mixture of methanol and water (30/70, v/v), which was filtered through 0.22 μm filters prior to use. The flow rate was set as 1.0 mL/min and the injection volume was 50 μL. The concentration of PMS (HSO_5^-) was analyzed on the same HPLC unit at 260 nm using a C18 reversed-phase column (250×3.0 mm) and a mixture of methanol (0.01 mL/min) and phosphoric acid buffer (0.24 mL/min of 0.3% H_3PO_4 in DI water) as mobile phase. The measurement of dissolved Cu and Fe ion was conducted on an ICP-MS (Agilent 7500, U.S). Total organic matter (TOC) values were obtained by a TOC/TN analyzer (Multi 3100, Analytik Jena, Germany). Chloride ion was analyzed through an ion chromatograph (ICS-3000, Dionex, U.S.) coupled with an AS-15 column (4×50 mm) and a DS6 conductivity detector.

RESULTS AND DISCUSSION

1. Synthesis and Characterization of $CuO\text{-}Fe_3O_4$ Nanoparticles

During the synthesis process, four samples were prepared with initial Fe/Cu molar ratios of 21.5 : 1 (sample 1, 5%$CuO\text{-}Fe_3O_4$), 14.0 : 1 (sample 2, 7.5%$CuO\text{-}Fe_3O_4$), 10.0 : 1 (sample 3, 10%$CuO\text{-}Fe_3O_4$), and 6.4 : 1 (sample 4, 15%$CuO\text{-}Fe_3O_4$). The preliminary experimental results showed that the copper content in different samples was

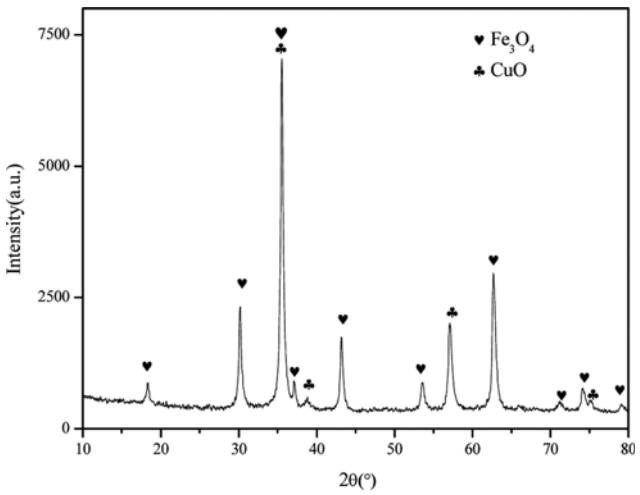

Fig. 1. XRD pattern of $CuO\text{-}Fe_3O_4$ nanocomposites (sample 1).

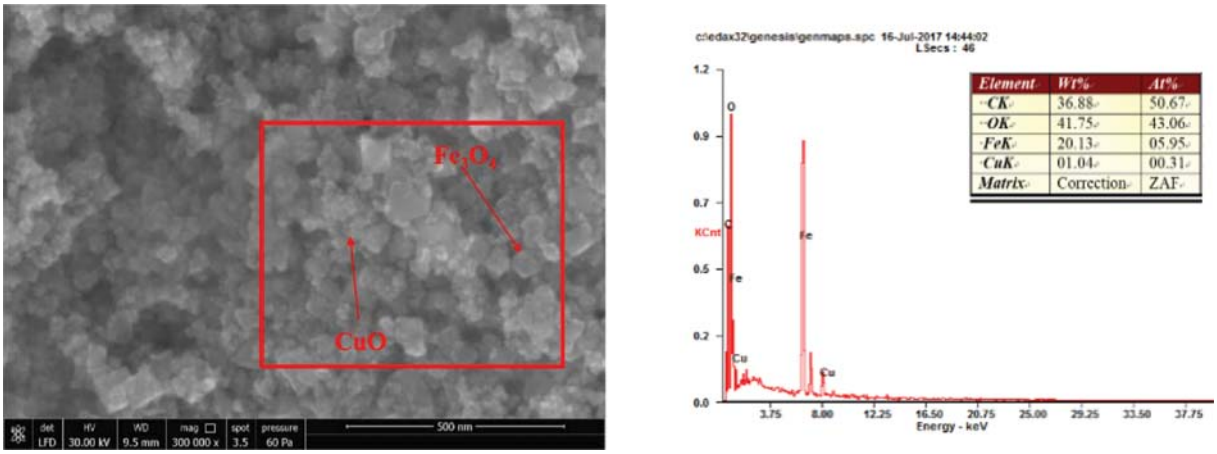

Fig. 2. SEM image and component molar ratio of CuO-Fe_3O_4 nanocomposites (sample 1).

expected to reach the designed value. All samples were only different in copper content, so sample 1 was set as an example to illustrate.

Fig. 1 shows the XRD pattern of 5%CuO-Fe_3O_4 at 2θ ranging from 10° to 80°, which clearly illustrates that the synthesized catalyst is highly crystalline. Some peaks matched well with face-centered cubic crystal of Fe_3O_4 (space group: Fd3m, JCPDs 88-0315), as evidenced by the diffraction peaks from (1 1 1), (2 2 0), (3 1 1), (2 2 2), (4 0 0), (4 2 2), (4 4 0), (6 2 0), (5 3 3) and (4 4 4). Other peaks corresponded to the planes of monoclinic crystal of CuO (space group: $C_2|c$, JCPDs 74-1021), as evidenced by the diffraction peaks from (–1 1 1), (1 1 1), (0 2 1) and (0 0 4). These results indicated that CuO-Fe_3O_4 catalysts were successfully prepared by a hydrothermal method.

The crystalline size can be evaluated on the basis of XRD patterns using Scherrer equation $D=K\lambda/(\beta\cos\theta)$, where K is the Scherrer constant (0.89), λ is the X-ray wavelength (0.15418 nm), β is the peak width at half maximum height and θ is the Bragg diffraction angle [35]. The average crystalline size of the spinel Fe_3O_4 and CuO crystals in the composites was calculated from the characteristic peaks-(311) for Fe_3O_4 crystal and (0 2 1) for CuO crystal. The crystalline size of Fe_3O_4 crystal and CuO crystal was 207 nm and 179 nm.

Seen from Fig. 2, the EDS spectra showed that the main elements of the synthesized nanoparticles were Fe, O and Cu. And the molar ratio of Fe to Cu was 21.95, which is approximately close to the designed value (21.5, 5%CuO-Fe_3O_4, sample 1).

The typical TEM and HRTEM images of the sample 1 (Fig. 3) indicated that the size of the synthesized nanoparticles was at nano-level, which was consistent with the XRD pattern. The distinct lattice fringes with spacings of 0.29 nm and 0.24 nm, which can be attributed to the coexisting Fe_3O_4 and CuO, respectively.

As shown in Fig. 4, the magnetic curves for sample 1 were measured at room temperature. The *S*-like magnetization hysteresis loop of the CuO-Fe_3O_4 nanoparticles suggested that the composites were superparamagnetic. The saturation magnetization of sample 1 was 75 emu/g, which indicated that the synthesized nanoparticles could easily be separated and reused from the aqueous solution by using an external magnet, which was attributed to its excellent magnetic property.

2. Catalytic Oxidation of 4-CP by CuO-Fe_3O_4 Nanoparticles

The efficiency of different systems to activate Oxone solution for the degradation of 4-CP was compared. The variation of 4-CP concentration with time is demonstrated in Fig. 5.

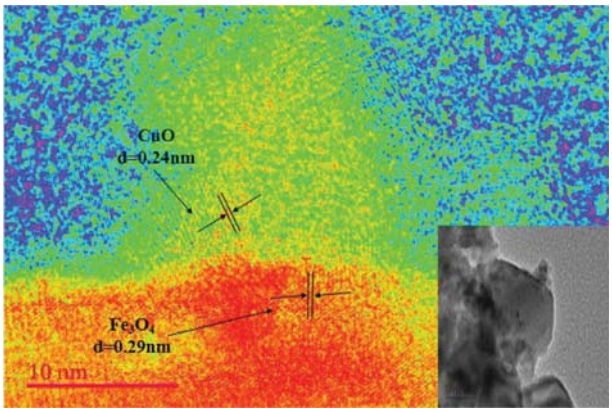

Fig. 3. TEM image of CuO-Fe_3O_4 nanocomposites (sample 1).

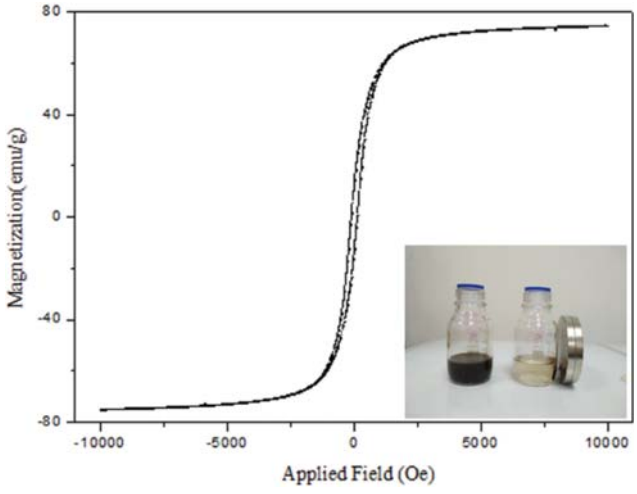

Fig. 4. *M-H* hysteresis loop of CuO-Fe_3O_4 nanocomposites at 300 K (sample 1). The inset shows photographs of the dispersion before and after recycling by magnetic separation for 1 min.

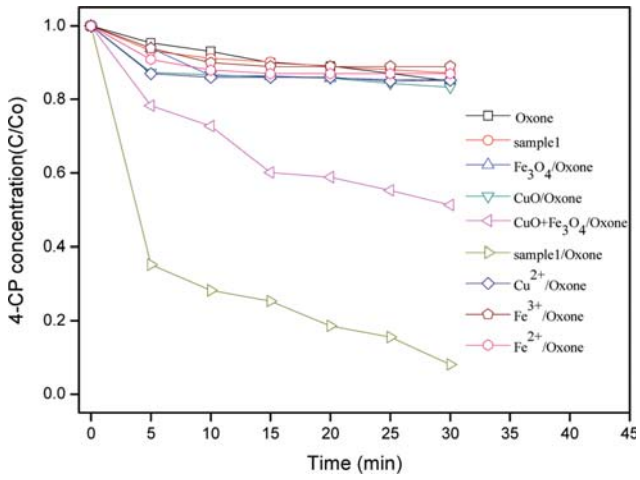

Fig. 5. 4-CP degradation in different system. Reaction conditions: catalyst dose=500 mg/L; c(Cu^{2+})=400 mg/L; c(Fe^{3+})=400 mg/L; c(Fe^{2+})=400 mg/L; Oxone dose=8 mM; T=303 K; initial 4-CP concentration=50 mg/L; 25 mM tetraborate buffered pH 8.5.

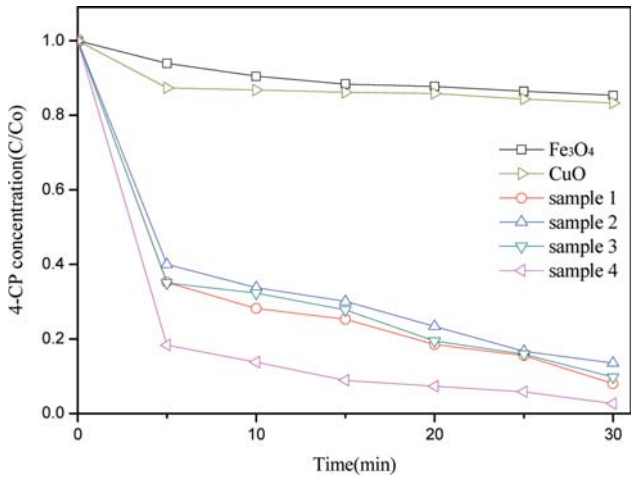

Fig. 6. 4-CP degradation on CuO-Fe_3O_4 nanoparticles with various Fe/Cu molar ratio. Reaction conditions: catalyst dose=500 mg/L; Oxone dose=8 mM; T=303 K; initial 4-CP concentration=50 mg/L; 25 mM tetraborate buffered pH 8.5.

The results in Fig. 5 show that PMS only led to a slight removal of 4-CP within 30 min. In absence of Oxone, a small amount of 4-CP diminished by sample 1 was primarily ascribed to the surface adsorption of CuO-Fe_3O_4 nanoparticles, which was negligible compared to the fast removal of 4-CP by heterogeneous Fenton reaction. Previous studies showed that Fe_3O_4 could activate PMS to oxidize Acid Orange 7 and acetaminophen [12,36]. The addition of Fe_3O_4 into the aqueous solution containing 4-CP and PMS enhanced the degradation of 4-CP a little, approximately 14.7% 4-CP reduction observed.

The 4-CP degradation was slightly promoted with the addition of CuO, about 16.7% 4-CP eliminated in the CuO/Oxone system. Although PMS was hardly activated with pure Fe_3O_4 or pure CuO, CuO-Fe_3O_4 nanoparticles had a better catalytic activity. Absolute majority of 4-CP was achieved to remove in 30 min with the Sample 1/Oxone coupled process. Furthermore, the physical mixture of CuO (25 mg/L) and Fe_3O_4 (475 mg/L) crystals with PMS was investigated. The removal efficiency of 4-CP in 30 min was 48.7%, lower than Sample 1/Oxone, but higher than CuO/Oxone and Fe_3O_4/Oxone. The results demonstrated that compared with CuO/Oxone, Fe_3O_4/Oxone and CuO+Fe_3O_4/Oxone (physical mixture), the catalytic capacity of sample 1/Oxone system was higher than that of mixture or pure crystals, suggesting that there might be a synergetic effect in the composite, thereby enhancing the relative rates of mass transfer to reactive sites and chemical reaction at reactive sites. In addition, a homogeneous catalytic system was also constructed to evaluate the catalytic degradation effect of copper ion, iron ion and ferrous ion. The results from Fig. 5 indicated that the activation of PMS occurred over the solid surface heterogeneously rather than homogeneously conducted by dissolved metal ion.

The degradation of 4-CP by different systems was compared. To explain the reasons for the good degradation effect of CuO-Fe_3O_4/PMS system, we calculated the activation energy (E_a) for the reaction. The degradation kinetics of 4-CP at different temperature (283 K, 293 K, 303 K and 313 K) was investigated. The E_a of the reaction on CuO-Fe_3O_4 surface was evaluated by plotting ln k against 1/T on the basis of Arrhenius equation and was determined as 35.82 kJ/mol. This value was higher than the activation energy of the diffusion-controlled reactions, which usually ranged within 10-13 kJ/mol, implying that the reaction rate was dominated by the rate of intrinsic chemical reactions on the oxide surface rather than the rate of mass transfer [37].

3. Effect of Various Fe/Cu Molar Ratios

The as-synthesized four samples with different Fe/Cu molar ratio, pure Fe_3O_4 and pure CuO were all applied to activate PMS for 4-CP degradation. The results in Fig. 6 show that the 4-CP removal efficiency of different catalysts was 92.0% (sample 1), 86.5% (sample 2), 90.3% (sample 3) and 94.3% (sample 4), respectively. The CuO content in the nanoparticles had a tremendous effect on the degradation of 4-CP. It was also seen that 4-CP removal efficiency would not increase significantly for the case of pure Fe_3O_4 or pure CuO as catalyst.

In all the studies cases, the 4-CP degradation process was simulated by a pseudo-first order kinetic model, being expressed as $\ln(C/C_o)=-kt$, where C and C_o were 4-CP concentrations (mg/L) at time of t=0 and t=t, k is the pseudo-first order rate constant (min^{-1}) and t is reaction time (min). By fitting with the kinetic model, the k values for the degradation of 4-CP in the system of sample 1, sample 2, sample 3, sample 4, Fe_3O_4 and CuO were 0.0673, 0.0600, 0.0669, 0.0831, 0.0050 and 0.0060 min^{-1}, respectively. After simple calculation, it was clearly seen that the k value in the system of sample 1 was 13 and 11 times that of single Fe_3O_4 and CuO, respectively. Such a great difference between k values in above systems strongly suggests that there is a synergistic effect between CuO and Fe_3O_4 in the CuO-Fe_3O_4 nanoparticles.

4. Effect of pH

The degradation of 4-CP was studied in the solution pH range of 5.5 to 13.0, and the results are shown in Fig. 7. As can be seen, in the sample 1/PMS system, the removal efficiency of 4-CP was

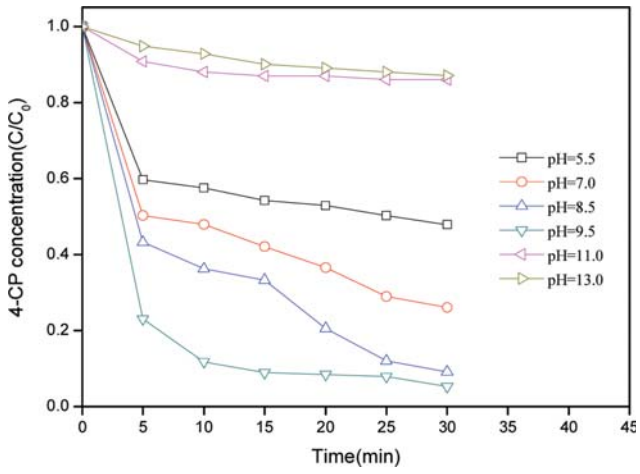

Fig. 7. Influence of pH on 4-CP degradation. All of the solution pH was adjusted with 25 mM tetraborate buffered. Reaction conditions: catalyst dose (sample 1)=500 mg/L; Oxone dose=8 mM; T=303 K; initial 4-CP concentration=50 mg/L.

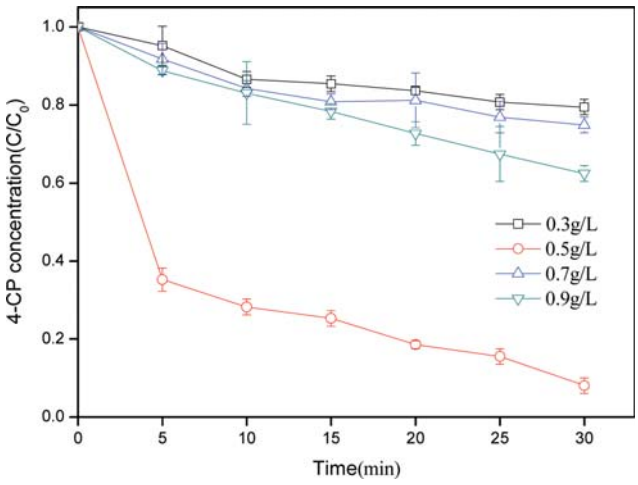

Fig. 8. Influence of catalyst dose on 4-CP degradation. The catalyst used in these experiments was sample 1. Reaction conditions: Oxone dose=8 mM; T=303 K; initial 4-CP concentration=50 mg/L; 25 mM tetraborate buffered pH 8.5.

52.1%, 73.9%, 90.9%, 94.7%, 14.0% and 12.8% when the initial solution pH was 5.5, 7.0, 8.5, 9.5, 11.0 and 13.0, respectively. It was observed that catalytic oxidation of 4-CP by CuO-Fe_3O_4/PMS system showed a dependence on initial pH. 4-CP degradation was enhanced as the initial pH increased from 5.5 to 9.5, and then declined from 9.5 to 13.0. The results indicated that 4-CP could be degraded efficiently in the sample 1/PMS system over a wide pH range, which is an obvious advantage over conventional Fenton reaction, which only could be carried out under strongly acidic condition (pH=2-3.5) [38]. The reason was mainly attributed to the influence of the solution pH on the pH_{pzc} and catalytic property of metal oxides. George [39] suggested that the surface charge of metal oxides was highly dependent on the relationship between the solution pH and pH_{pzc} of metal oxides. At pH<pH_{pzc}, the surface charge of metal oxides was positive while negative at pH> pH_{pzc}. Ren et al. [40] found that heterogeneous catalytic ozonation by $NiFe_2O_4$ showed the maximum degradation efficiency was around pH_{pzc} of the catalyst. Since the pH_{pzc} of CuO and Fe_3O_4 was around 9.5 and 6.5, respectively, however, the pH_{pzc} of CuO-Fe_3O_4 nanoparticles was measured as 8.5. Besides, the pKa of PMS was 9.4. Thus, in the investigated pH range of 5.5-13.0, the existed form of PMS depended mainly on solution pH and the second pKa [41]. Obviously, the CuO-Fe_3O_4 nanoparticles were positively charged in wide pH range (pH<9.0). Meanwhile, the existing form of PMS was $\cdot HSO_5^-$ at acid and neutral conditions (5.5<pH<9.5) and $\cdot SO_5^-$ at pH range of 9.5 to 13.0. When pH remained above 8.5, the surface of CuO-Fe_3O_4 nanoparticles was negatively charged, repulsive force from electrostatic charge reduced the interaction chance between PMS and CuO-Fe_3O_4 nanoparticles, resulting in the decline of 4-CP degradation. With the decrease of pH (pH<9.0), the surfaces of CuO-Fe_3O_4 nanoparticles would be positively charged and facilitate the contact between PMS and CuO-Fe_3O_4 nanoparticles by attractive force, but the degradation efficiency of 4-CP declined. The results indicated that the hydroxyl groups on CuO-Fe_3O_4 nanoparticles surface in neutral state played an important role in PMS activation process. Furthermore, the degradation efficiency of 4-CP at pH 9.5 was higher than that at pH≤8.5, which indicated that $\cdot SO_5^-$ was easier to be activated than $\cdot HSO_5^-$ in heterogeneous catalytic oxidation [42].

5. Effect of Catalyst Dosage and Oxidant Dosage

The effect of the catalyst dosage on the 4-CP removal efficiency is illustrated in Fig. 8. According to the results, at the catalyst dosage of 0.3-0.5 g/L, the increase of the catalyst dosage resulted in an increase of 4-CP degradation while decline at the catalyst dosage of 0.7-0.9 g/L. The highest degradation efficiency was achieved at the dosage of 0.5 g/L, not 0.9 g/L, which was likely because of the agglomeration of nanoparticles, the diffusion limitation phenomenon in heterogeneous reactions and self-quenching of reactive oxygen species generated in a short time. There have been some studies that could confirm the above speculations. Xu et al. [43] investigated the influence of Fe_3O_4/CeO_2 addition on the degradation of 4-CP. They observed that the removal rate constant increased with an increasing amount of Fe_3O_4/CeO_2 from 1.0 to 2.0 g/L and then slight decreased. They speculated that the enhancement of 4-CP removal might be ascribed to the increasing amount of active sites for the formation of ·OH, and the slight decrease of 4-CP removal might be attributed to the agglomeration of nanoparticles and the scavenging of ·OH by excess Fe^{2+}. El Zein et al. [44] studied the kinetics and products of the reaction of HONO with solid film of Fe_2O_3 and Arizona Test Dust (ATD). They found that the initial uptake of HONO was not expected to be dependent on the gas phase concentration of the reactant, since at the initial stage of the surface exposure, the active sites on the catalyst's surface were not depleted and were all available for the heterogenous reaction. However, diffusion limitation influenced the reaction rate between HONO, Fe_2O_3 and ATD. Yan's group [45] has focused on the Fe_3O_4/PS system for sulfamonomethoxine (SMM) degradation. As they have stated, when Fe_3O_4 was added in excess, an excess of $\cdot SO_4^-$ species were generated, resulting in disappearance of $\cdot SO_4^-$ species without the decomposition of SMM due to the combination between

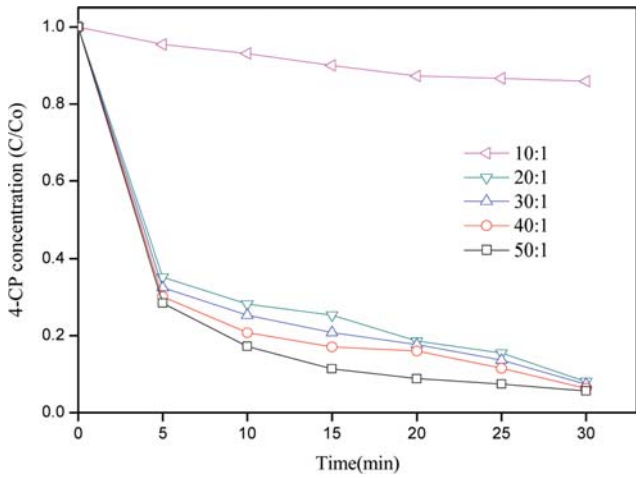

Fig. 9. Influence of PMS/4-CP molar ratio on 4-CP degradation. Reaction conditions: catalyst dose (sample 1)=500 mg/L; T=303 K; initial 4-CP concentration=50 mg/L; 25 mM tetraborate buffered pH 8.5.

$\cdot SO_4^-$ species themselves. Moreover, the interaction between excess Fe^{2+} on the surface of Fe_3O_4 and $\cdot SO_4^-$ might directly quench $\cdot SO_4^-$.

Fig. 9 shows the effect of Oxone concentration on 4-CP degradation. The degradation of 4-CP was conducted at the Oxone/4-CP molar ratio from 10 : 1 to 50 : 1. As the dosage of Oxone increased, the removal efficiency of 4-CP increased greatly. Results revealed that Oxone was decomposed at the surface of catalyst to generate the reactive radicals. Thus, the increase of Oxone concentration would lead to producing more radicals. However, the plateau was reached at the Oxone/4-CP molar ratio of 20 : 1 in solution; further increase in Oxone concentration would not significantly improve the degradation efficiency.

6. Mineralization of 4-CP and Dechlorination

The mineralization level of 4-CP in CuO-Fe_3O_4/PMS system was evaluated through the degree of TOC removal and the determination of chlorine ions content in the solution. As seen in Fig. 10, 57% of TOC removal was reached within 30 min. Xu et al. [46] suggested that the residual TOC might associate with some small molecular organic acids generated from the catalytic reaction. The concentration of chloride ion was analyzed by ion chromatograph. During the reaction process, about 78.5% of Cl was released into the solution.

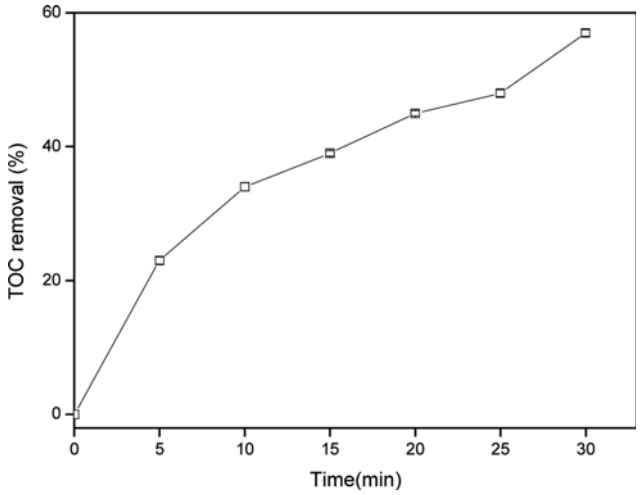

Fig. 10. TOC removal during the catalytic degradation process.

7. Stability and Reusability of the Catalysts

To evaluate the stability of CuO-Fe_3O_4 nanoparticles, the leaching of Cu^{2+} and Fe^{3+} was measured during the degradation process of 4-CP with the addition of 500 mg/L catalysts. It was obviously found that under the reaction conditions, ICP analysis showed that Cu^{2+} leaching was about 0.2115 mg/L in 30 min, accounting for approximately 1% of the total Cu content of the catalyst while the Fe^{3+} leaching was 0.8973 mg/L, accounting for 0.26% of the total Fe content of the catalyst. Moreover, the recycled catalyst was carried out during the degradation process of 4-CP. After the reaction time was finished, the used catalyst was collected by vacuum filtration, washed with DI water and ethanol several times, and mixed with the fresh 4-CP solution. Then 8 mM PMS was added and the second cycle of the reaction was conducted. These steps were repeated several times. After the fifth run, the 4-CP degradation efficiency was still about 85%, which indicated that CuO-Fe_3O_4 nanoparticles has an excellent stability (Fig. 11).

8. Identification of the Reaction Mechanism

Metal-catalyzed activation of PMS usually generated four main types of reactive radical, including sulfate radicals ($\cdot SO_4^-$), hydroxyl radicals ($\cdot OH$), peroxysulfate radicals ($\cdot SO_5^-$) and singlet oxygen ($^1O_2$) [47]. To identify the dominating radical species in CuO-Fe_3O_4/PMS system, quenching experiments were conducted. Methanol (MeOH) and *tert*-butanol (TBA) were selected as quenching agents since MeOH was a popular radical quencher for $\cdot OH$ ($k=9.7\times10^8\ M^{-1}\cdot s^{-1}$) and $\cdot SO_4^{-1}$ ($k=2.5\times10^7\ M^{-1}\cdot s^{-1}$), while TBA was effective to quench $\cdot OH$ ($k=3.8\text{-}7.6\times10^8\ M^{-1}\cdot s^{-1}$) [48]. In addition, Nie et al. [34] investigated the radical species formed in the Cu^0-Fe_3O_4/PMS system and found that singlet oxygen ($^1O_2$) was also one type

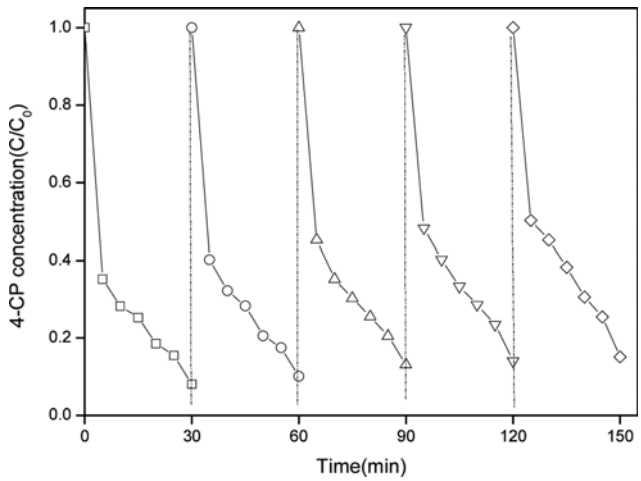

Fig. 11. Degradation kinetics of 4-CP using the recycled catalysts. Reaction conditions: catalyst dose (sample 1)=500 mg/L; Oxone dose=8 mM; T=303 K; initial 4-CP concentration=50 mg/L; 25 mM tetraborate buffered pH 8.5.

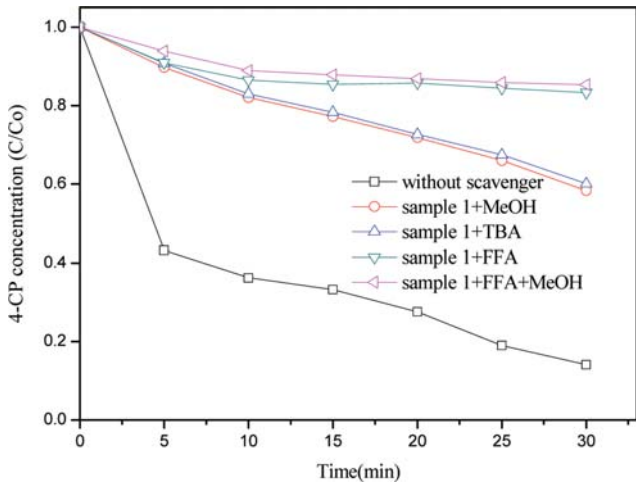

Fig. 12. Influence of quenching agents, MeOH (100 mM), TBA (100 mM), FFA (100 mM) and FFA+MeOH (200 mM) on 4-CP degradation. Reaction conditions: catalyst dose (sample 1)= 500 mg/L; Oxone dose=8 mM; T=303 K; initial 4-CP concentration=50 mg/L; 25 mM tetraborate buffered pH 8.5.

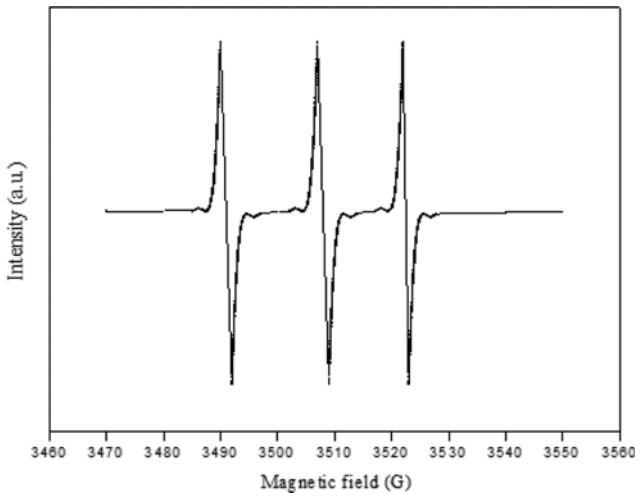

Fig. 14. Tetramethylpiperidine spin-trapping electron spin resonance spectrum of $^1O_2$. Reaction conditions: catalyst dose (sample 1)=500 mg/L; Oxone dose=8 mM; T=303 K; 25 mM tetraborate buffered pH 8.5; TEMP=20 mM.

of major reactive radical. Thus, furfuryl alcohol (FFA) was used as scavenger of $^1O_2$ ($k=1.2\times10^8\ M^{-1}\cdot s^{-1}$) and ·OH ($k=1.5\times10^{10}\ M^{-1}\cdot s^{-1}$), but had no quenching effect on $\cdot SO_4^-$ [49,50]. As shown in Fig. 12, the addition of 200 mM FFA+MeOH greatly decreased the 4-CP removal efficiency to 14.6%, mainly attributed to the adsorption effect of 4-CP on the CuO-Fe_3O_4 nanoparticles, which indicated that FFA+MeOH almost completely inhibited the 4-CP degradation in the sample 1/Oxone system. At the same time, the addition of 100 mM FFA obviously inhibited the reduction of 4-CP (16.7%). This apparently hinted that $^1O_2$ and ·OH were the main reactive oxygen species produced in sample 1/Oxone system; meanwhile there still existed a very small amount of sulfate radical. The presence of 100 mM TBA or 100 mM MeOH also moderately depressed the 4-CP degradation from the previous 86.0% removal in 30 min to 40.0% and 41.7% removal of 4-CP, respectively. Thus, it could be concluded that ·OH played an important role in the removal of 4-CP without taking into account the adsorption of the catalyst. In summary, $^1O_2$ played a major role while ·OH played an important role, while a small amount of $\cdot SO_4^-$ also played a role in certain degree in 4-CP removal process. The generation of $^1O_2$, ·OH and $\cdot SO_4^-$ radicals in the sample 1/Oxone system were further confirmed by ESR analysis.

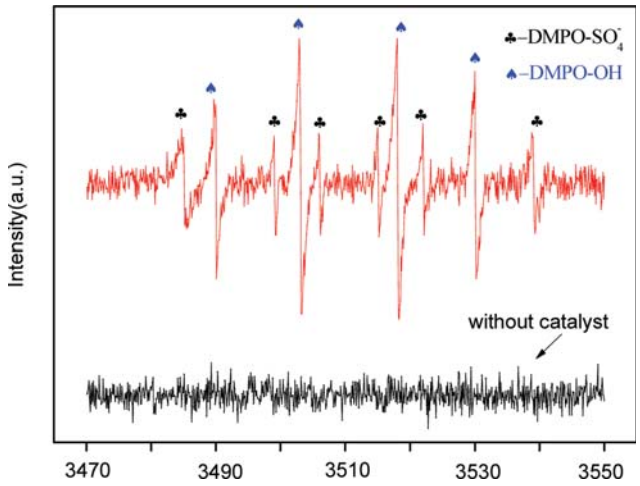

Fig. 13. 5,5-Dimethyl-pyrroline-N-oxide (DMPO) spin-trapping electron spin resonance spectrum of ·OH and $\cdot SO_4^-$. Reaction conditions: catalyst dose (sample 1)=500 mg/L; Oxone dose= 8 mM; T=303 K; 25 mM tetraborate buffered pH 8.5; DMPO= 20 mM.

ESR technology was used to confirm the generation of $^1O_2$, ·OH and $\cdot SO_4^-$ radicals. As shown in Fig. 13, a typical six-peak spectrum of DMPO-·SO_4 and four-peak spectrum of DMPO-·OH was detected in the CuO-Fe_3O_4/PMS system, indicating that ·OH and $\cdot SO_4^-$ were generated in this system. In addition, Fig. 14 shows a typical triplet signal of TEMP-$^1O_2$ which further confirms that $^1O_2$ was also generated in CuO-Fe_3O_4/PMS system. Some studies have reported that PMS could be activated via a non-radical pathway to generate $^1O_2$ in heterogenous catalytic process. Liu et al. [51] first explored activity of sillenite $Bi_{25}FeO_{40}$ for decomposition of PMS to oxidize levofloxacin. They reported that $^1O_2$ was identified as the main reactive oxygen species through radical scavenging experiments, EPR experiment and HPLC-MS determination. Zhou et al. [52] first investigated the reactions between PMS and benzoquinone (BQ). They stated that BQ could effectively activate PMS to generate $^1O_2$ for the degradation of sulfamethoxazole (SMX). Interestingly, quenching studies suggested that neither $\cdot SO_4^-$ nor ·OH was produced therein. Ahmadi et al. [53] made some effects to present an efficient method for PMS activation. They utilized UVC-LEDs and US to activate PMS for decolorization of Direct Orange 26 (DO26). Scavenging experiments showed that $^1O_2$, $\cdot SO_4^-$ and ·OH contributed in the degradation of DO26.

To better understand the roles of Fe and Cu species in the activation of PMS, the XPS spectra of CuO-Fe_3O_4 nanoparticles were recorded before and after the degradation experiments. As shown

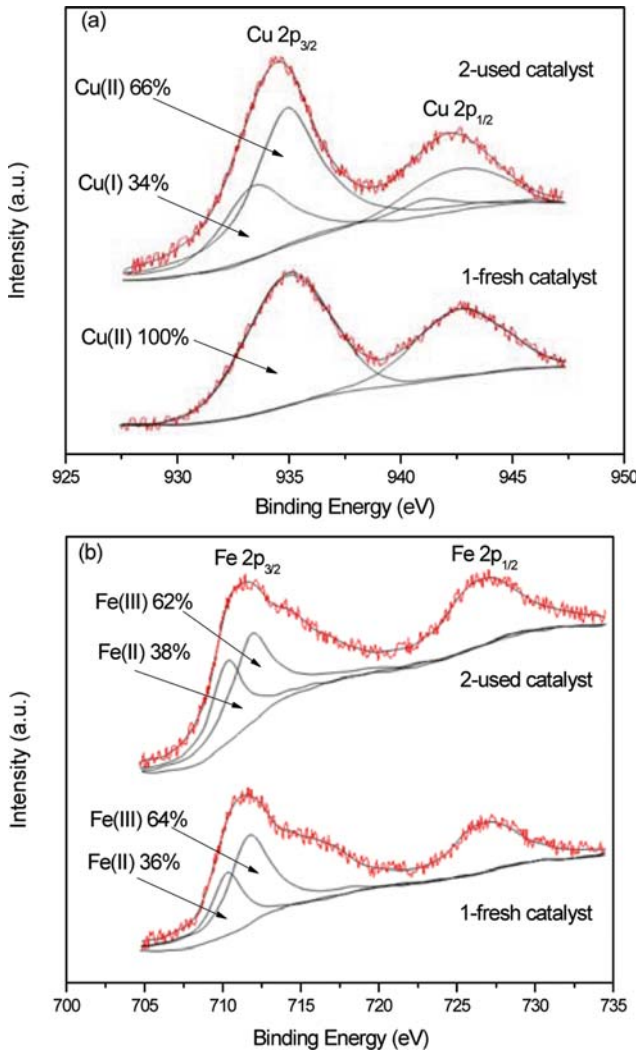

Fig. 15. (a) Cu 2p and (b) Fe 2p XPS envelop of (1) the fresh and (2) used CuO-Fe_3O_4 nanocomposites (sample 1).

in Fig. 15, the peaks of Cu 2p3/2 and Fe 2p3/2 were at 934.0 eV and 712.3 eV for the fresh CuO-Fe_3O_4 nanoparticles, which were assigned to Cu(II) and Fe(III). After the catalytic degradation of 4-CP, the binding energy values of Cu 2p3/2 and Fe 2p3/2 slightly declined (933.5 eV for Cu and 711.1 eV for Fe), which indicated that the valence of Cu and Fe species was a mixture. Based on the deconvolution of Cu 2p and Fe 2p envelop, Cu(I) and Fe(II) accounted for 34% and 38%, respectively, which indicated that Cu(II) and Fe(III) on the surface of the used catalyst were transformed partially to Cu(I) and Fe(II), respectively.

According to the above experimental results, the possible mechanism for the activation of PMS on CuO-Fe_3O_4 nanoparticles was proposed as summarized by reactions (1)-(13).

$$\equiv Cu^{I}\text{-}OH + \bullet HSO_5^- \rightarrow \equiv Cu^{II}\text{-}OOSO_3^- + H_2O \quad (1)$$

$$\equiv Cu^{II}\text{-}OOSO_3^- + H_2O \rightarrow \bullet SO_5^- + \equiv Cu^{I}\text{-}OH + H^+ \quad (2)$$

$$\equiv Cu^{I}\text{-}OH + \equiv Fe^{III}\text{-}OH \rightarrow \equiv Cu^{II}\text{-}OH + \equiv Fe^{II}\text{-}OH \quad (3)$$

$$\equiv Cu^{I}\text{-}OH + \bullet HSO_5^- \rightarrow \equiv Cu^{I}\text{-}OOSO_3^- + H_2O \quad (4)$$

$$\equiv Cu^{I}\text{-}OOSO_3^- + H_2O \rightarrow \bullet SO_4^- + \equiv Cu^{II}\text{-}OH + OH^- \quad (5)$$

$$\equiv Fe^{II}\text{-}OH + \bullet HSO_5^- \rightarrow \equiv Fe^{II}\text{-}OOSO_3^- + H_2O \quad (6)$$

$$\equiv Fe^{II}\text{-}OOSO_3^- + H_2O \rightarrow \bullet SO_4^- + \equiv Fe^{III}\text{-}OH + OH^- \quad (7)$$

$$\bullet SO_4^- + H_2O \rightarrow \bullet OH + H^+ + SO_4^{2-} \quad (8)$$

$$\bullet SO_4^-/\bullet OH + 4\text{-CP} \rightarrow \text{intermediate} \quad (9)$$

$$\bullet HSO_5^- + H_2O \xrightarrow[OH^-]{catalyst} HO_2^- + SO_4^{2-} + 2H^+ \quad (10)$$

$$HO_2^- + \bullet HSO_5^- \rightarrow \bullet OH + SO_4^{2-} + \bullet O_2^- + H^+ \quad (11)$$

$$2\bullet O_2^- + H_2O \rightarrow {}^1O_2 + H_2O_2 + 2OH^- \quad (12)$$

$${}^1O_2 + 4\text{-CP} \rightarrow \text{intermediate} \quad (13)$$

First, PMS could be activated by a radical pathway. PMS initially conjuncted with CuO and then generated $\cdot SO_5^-$, while Cu (II) was reduced to Cu (I) (Eq. (1)-(2)). Then, the Cu (I) species may have given electrons to Fe (III) in Fe_3O_4 and transferred to Cu (II) in CuO because the standard redox potential of Fe^{3+}/Fe^{2+} (0.77 V) was higher than Cu^{2+}/Cu^+ (0.17 V) (Eq. (3)). Hence, the transfer of electrons from Cu^+ to Fe^{3+} was thermodynamically favored. The results revealed that there existed a synergistic effect between copper oxide and ferroferric oxide in the CuO-Fe_3O_4 nanoparticles. Additionally, some of the Cu (I) species might adhere with $\cdot HSO_5^-$ and be oxidized to Cu (II), while $\cdot SO_4^-$ was released into the solution (Eqs. (4)-(5)). Furthermore, the generated Fe (II) formed complex with $\cdot HSO_5^-$ (Eq. (6)) and to be oxidized to Fe (III), releasing $\cdot SO_4^-$ into the solution (Eq. (7)). Finally, the $\cdot SO_4^-$ could react with H_2O to produce ·OH (Eq. (8)). Because of high oxidation potential, the generated $\cdot SO_4^-$ and ·OH would attack 4-CP molecule, which was responsible for the 4-CP degradation (Eq. (9)).

PMS could also be activated by a non-radical pathway through partial activation of PMS. Because of electrostatic interaction, $\cdot HSO_5^-$ was absorbed on the surface of the catalyst. Previous studies showed that Cu (II) played an important role in partial activation of PS or PMS, mainly due to its special external valence electron arrangement [29,54]. Specially, the d orbit of Cu (II) could be coordinated with the unpaired electron of $\cdot HSO_5^-$. Under the action of the catalyst, $\cdot HSO_5^-$ reacted with H_2O, and then HO_2^- was generated and released into the solution (Eq. (10)). Then, the HO_2^- could react with the adsorbed $\cdot HSO_5^-$ on the surface of the catalyst to produce $\cdot O_2^-$ (Eq. (11)). Li et al. [55] suggested that superoxide radical was the most important precursor for the generation of singlet oxygen. Finally, the generated $\cdot O_2^-$ could react with H_2O to form $^1O_2$ (Eq. (12)). The results showed that $^1O_2$ was the major ROS in the non-radical activation of PMS for 4-CP degradation.

Based on the radical scavenging and ESR trapping results obtained in this study, a possible mechanism for PMS activation by CuO-Fe_3O_4 nanoparticles and 4-CP degradation is proposed in Fig. 16.

CONCLUSION

Magnetic CuO-Fe_3O_4 nanoparticles with low cost and little hazard were synthesized through one-pot hydrothermal method, then used as heterogeneous catalysts to activate PMS for 4-CP degradation. Markedly higher activity of sample 1 with 5% CuO content

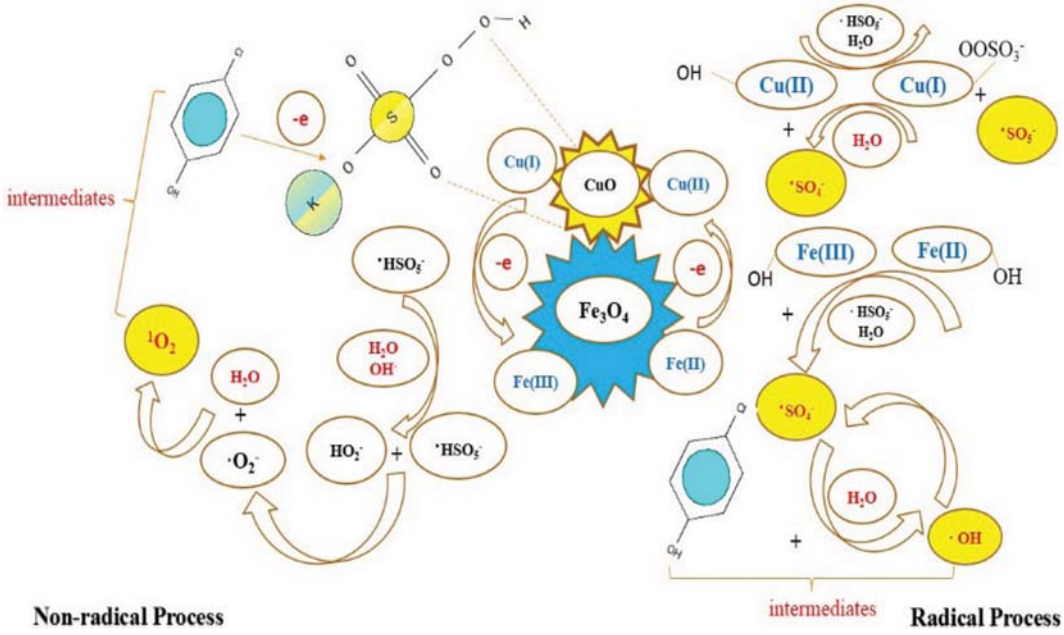

Fig. 16. The proposed catalytic oxidation mechanism in CuO-Fe_3O_4/PMS system.

of the nanoparticles was observed towards the degradation of 4-CP in the presence of CuO-Fe_3O_4 in comparison with the use of pure CuO and pure Fe_3O_4 as catalysts. The catalyst showed stability in element valence, crystallinity and catalytic activity during the successive repeated reactions. The high catalytic activity of the CuO-Fe_3O_4 nanoparticles was attributed to the synergistic effect of CuO and Fe_3O_4 crystals. Both $^1O_2$, ·OH and $\cdot SO_4^-$ radicals were suggested as the main reactive oxygen species in CuO-Fe_3O_4/PMS system, which indicated that PMS was activated through a radial and non-radical process. The catalytic mechanism was proposed according to quenching experiments and ESR spectra. These results revealed that CuO-Fe_3O_4 nanoparticles were effective, environmentally friendly and low cost catalysts for efficient activation of reactive oxygen species from PMS to degrade refractory organic pollutants. They hold great potential in the oxidative treatment of industrial waste and contaminated water.

ACKNOWLEDGEMENT

This work was supported by the National Natural Science Foundation of China (No. 51508564), Graduate Research and Innovation Project of Chongqing City (No. CYB16126 & CYS17301) and Navy Logistics Research Project (No. CHJ13J021).

REFERENCES

1. M. Pera-Titus, V. GarcíA-Molina, M. A. Baños, J. Giménez and S. Esplugas, *Appl. Catal. B Environ.*, **47**, 219 (2004).
2. Y. Hwang, P. D. Mines, M. H. Jakobsen and H. R. Andersen, *Appl. Catal. B Environ.*, **166-167**, 18 (2015).
3. M. Cheng, W. Ma, J. Li, Y. P. Huang and J. Zhao, *Environ. Sci. Technol.*, **38**, 1569 (2004).
4. J. Xu, W. Wang, E. Gao, J. Ren and L. Wang, *Catal. Commun.*, **12**, 834 (2011).
5. I. Oller, S. Malato and J. A. Sánchez-Pérez, *Sci. Total Environ.*, **409**, 4141 (2012).
6. H. Sun, S. Liu, G. Zhou, H. M. Ang, M. O. Tadé and S. Wang, *ACS Appl. Mater. Inter.*, **4**, 5466 (2012).
7. Y. Xiao, L. Zhang, Z. Wei, K. Y. Lim, R. D. Webster and T. T. Lim, *Water Res.*, **102**, 629 (2016).
8. M. M. Ahmed and S. Chiron, *Water Res.*, **48**, 229 (2014).
9. G. P. Anipsitakis and D. D. Dionysiou, *Environ. Sci. Technol.*, **38**, 3705 (2004).
10. R. H. Waldemer, P. G. Tratnyek, R. L. Johnson and J. T. Nurmi, *Environ. Sci. Technol.*, **41**, 1010 (2007).
11. Y. H. Guan, J. Ma, X. C. Li, J. Fang and L. Chen, *Environ. Sci. Technol.*, **45**, 9308 (2011).
12. N. Wang, L. Zhu, M. Wang, M. Wang, D. Wang and H. Tang, *Ultrason. Sonochem.*, **17**, 78 (2010).
13. O. S. Furman, A. L. Teel and R. J. Watts, *Environ. Sci. Technol.*, **44**, 6423 (2010).
14. H. Sun, H. Liang, G. Zhou and S. Wang, *J. Colloid Interface Sci.*, **394**, 394 (2013).
15. M. Ahmad, A. L. Teel and R. J. Watts, *J. Contam. Hydrol.*, **115**, 34 (2010).
16. A. L. Teel, M. Ahmad and R. J. Watts, *J. Hazard. Mater.*, **196**, 153 (2011).
17. P. R. Shukla, S. Wang, H. Sun, H. M. Ang and M. Tadé, *Appl. Catal. B Environ.*, **100**, 529 (2010).
18. E. Saputra, S. Muhammad, H. Sun, H. M. Ang, M. O. Tadé and S. Wang, *Environ. Sci. Technol.*, **47**, 5882 (2013).
19. X. Duan, H. Sun and S. Wang, *Accounts Chem. Res.*, **51**, 678 (2018).
20. E. Saputra, S. Muhammad, H. Sun and S. Wang, *RSC Adv.*, **3**, 21905 (2013).
21. P. Shao, X. Duan, J. Xu, J. Tian, W. Shi, S. Gao, M. Xu, F. Cui and S. Wang, *J. Hazard. Mater.*, **322**, 532 (2017).

22. C. Liu, M. Zhao, S. He, Z. Cao and W. Chen, *Desalin. Water Treat.*, **97**, 262 (2017).
23. Y. Leng, W. Guo, X. Shi, Y. Li, A. Wang, F. Hao and L. Xing, *Chem. Eng. J.,* **240**, 338 (2014).
24. Q. Tang, Y. Wang, J. Guo, P. Yang, X. Zhou and X. Lei, *Chinese J. Environ. Eng.*, **11**, 2084 (2017).
25. T. Zhang, Y. Chen, Y. Wang, R. Le, Y. Yang and J. P. Croué, *Environ. Sci. Technol.*, **48**, 5868 (2014).
26. F. Ji, C. Li and L. Deng, *Chem. Eng. J.*, **178**, 239 (2011).
27. P. Avetta, A. Pensato, M. Minella, M. Malandrino, V. Maurino, C. Minero, K. Hanna and D. Vione, *Environ. Sci. Technol.*, **49**, 15883 (2015).
28. J. Liu, J. Zhou, Z. Ding, Z. Zhao, X. Xiao and Z. Fang, *Ultrason. Sonochem.*, **34**, 953 (2017).
29. Y. Lei, C. S. Chen, Y. J. Tu, Y. Huang and H. Zhang, *Environ. Sci. Technol.*, **49**, 6838 (2015).
30. J. Liu, Z. Zhao, P. Shao and F. Cui, *Chem. Eng. J.*, **262**, 854 (2015).
31. G. Barzegar, S. Jorfi, V. Zarezade, M. Khatebasreh, F. Mehdipour and F. Ghanbari, *Chemosphere*, **201**, 370 (2018).
32. Y. Guo, Z. Zeng, Y. Li, Z. Huang and J. Yang, *Sep. Purif. Technol.*, **179**, 257 (2017).
33. T. Sun, Z. Zhao, Z. Liang, J. Liu, W. Shi and F. Cui, *J. Colloid Interface Sci.*, **495**, 168 (2017).
34. G. Nie, J. Huang, Y. Hu, Y. Ding, X. Han and H. Tang, *Chinese J. Catal.*, **38**, 227 (2017).
35. A. C. Nawle, A. V. Humbe, M. K. Babrekar, S. S. Deshmukh and K. M. Jadhav, *J. Alloy. Compd.*, **695**, 1573 (2017).
36. C. Tan, N. Gao, Y. Deng, J. Deng, S. Zhou, J. Li and X. Xin, *J. Hazard. Mater.*, **276**, 452 (2014).
37. X. Xue, K. Hanna, M. Abdelmoula and N. Deng, *Appl. Catal. B Environ.*, **89**, 432 (2009).
38. D. Häussler, M. Bartsch, M. Aindow, I. P. Jones and U. Messerschmidt, *Waste Manage.*, **32**, 1236 (2012).
39. G. A. Parks, *Chem. Rev.*, **65**, 177 (1965).
40. Y. Ren, Q. Dong, J. Feng, J. Ma, Q. Wen and M. Zhang, *J. Colloid Interface Sci.*, **382**, 90 (2012).
41. S. K. Rani, D. Easwaramoorthy, I. M. Bilal and M. Palanichamy, *Appl. Catal. A Gen.*, **369**, 1 (2009).
42. Y. H. Guan, J. Ma, Y. M. Ren, Y. Liu, J. Xiao, L. Lin and C. Zhang, *Water Res.*, **47**, 5431 (2013).
43. L. Xu and J. Wang, *Environ. Sci. Technol.*, **46**, 10145 (2012).
44. A. El Zein, M. N. Romanias and Y. Bedjanian, *Environ. Sci. Technol.*, **47**, 6325 (2013).
45. J. Yan, M. Lei, L. Zhu, M. N. Anjum, J. Zou and H. Tang, *J. Hazard. Mater.*, **186**, 1398 (2011).
46. L. Xu and J. Wang, *Appl. Catal. B Environ.*, **123-124**, 117 (2012).
47. F. Ghanbari and M. Moradi, *Chem. Eng. J.*, **102**, 307 (2017).
48. R. Yin, W. Guo, H. Wang, J. Du, X. Zhou, Q. Wu, H. Zheng, J. Chang and N. Ren, *Chem. Eng. J.*, **335**, 145 (2018).
49. E. Appiani, R. Ossola, D. E. Latch, P. R. Erickson and K. Mcneill, *Environ. Sci. Proc. Impact*, **19**, 507 (2017).
50. S. Mostafa and F. L. Rosarioortiz, *Environ. Sci. Technol.*, **47**, 8179 (2013).
51. Y. Liu, H. Guo, Y. Zhang, W. Tang, X. Cheng and W. Li, *Chem. Eng. J.*, **343**, 128 (2018).
52. Y. Zhou, J. Jiang, Y. Gao, J. Ma, S. Pang, J. Li, X. Lu and L. Yuan, *Environ. Sci. Technol.*, **49**, 12941 (2015).
53. M. Ahmadi and F. Ghanbari, *Environ. Sci. Pollut. R.*, **25**, 6003 (2018).
54. Z. Yang, D. Dai, Y. Yao, L. Chen, Q. Liu and L. Luo, *Chem. Eng. J.*, **322**, 546 (2017).
55. X. Li, J. Liu, A. I. Rykov, H. Han, C. Jin, X. Liu and J. Wang, *Appl. Catal. B Environ.*, **179**, 196 (2015).